NAVAL POSTGRADUATE SCHOOL
Monterey, California

THESIS

PROGRESSIVE FAILURE MODELING IN NOTCHED CROSS-PLY FIBROUS COMPOSITES

by

Linda E. Craugh

March 1999

Thesis Advisor: Young W. Kwon

Approved for public release; distribution is unlimited.

REPORT DOCUMENTATION PAGE

Form Approved OMB No. 0704-0188

1. AGENCY USE ONLY *(Leave blank)*	2. REPORT DATE	3. REPORT TYPE AND DATES COVERED
	March 1999	Master's Thesis

4. TITLE AND SUBTITLE
PROGRESSIVE FAILURE MODELING IN NOTCHED CROSS-PLY FIBROUS COMPOSITES

5. FUNDING NUMBERS

6. AUTHOR(S)
Craugh, Linda E.

7. PERFORMING ORGANIZATION NAME(S) AND ADDRESS(ES)
Naval Postgraduate School
Monterey, CA 93943-5000

8. PERFORMING ORGANIZATION REPORT NUMBER

9. SPONSORING / MONITORING AGENCY NAME(S) AND ADDRESS(ES)

10. SPONSORING / MONITORING AGENCY REPORT NUMBER

11. SUPPLEMENTARY NOTES
The views expressed in this thesis are those of the author and do not reflect the official policy or position of the Department of Defense or the U.S. Government.

12a. DISTRIBUTION / AVAILABILITY STATEMENT
Approved for public release; distribution is unlimited.

12b. DISTRIBUTION CODE

13. ABSTRACT *(maximum 200 words)*

The objective of this study was to model and simulate progressive failure initiating from a notch tip in a laminated fibrous composite subjected to tensile in-plane loading. The micro/macro-level approach was used for this study. The micro-level analysis used the 3-D unit cell model while macro-level analysis used the finite element analysis technique. A cross-ply laminate with double-edge notches was studied to investigate delamination, fiber splitting, and transverse matrix cracking in the structure. Numerical results were compared to previous experimental work.

14. SUBJECT TERMS	15. NUMBER OF PAGES
Finite Element Method, Composite Micromechanics, Delamination	58
	16. PRICE CODE

17. SECURITY CLASSIFICATION OF REPORT	18. SECURITY CLASSIFICATION OF THIS PAGE	19. SECURITY CLASSIFI- CATION OF ABSTRACT	20. LIMITATION OF ABSTRACT
Unclassified	Unclassified	Unclassified	UL

NSN 7540-01-280-5500

Standard Form 298 (Rev. 2-89)
Prescribed by ANSI Std. 239-18

THIS PAGE INTENTIONALLY LEFT BLANK

Approved for public release; distribution is unlimited

PROGRESSIVE FAILURE MODELING IN NOTCHED CROSS-PLY FIBROUS COMPOSITES

Linda E. Craugh
Lieutenant, United States Navy
B.S., Cornell University, 1991

Submitted in partial fulfillment of the
requirements for the degree of

MASTER OF SCIENCE IN MECHANICAL ENGINEERING

from the

NAVAL POSTGRADUATE SCHOOL
March 1999

Author: LLEC
Linda E. Craugh

Approved by:
Young W. Kwon, Thesis Advisor

Terry R. McNelley, Chairman
Department of Mechanical Engineering

THIS PAGE INTENTIONALLY LEFT BLANK

ABSTRACT

The objective of this study was to model and simulate progressive failure initiating from a notch tip in a laminated fibrous composite subjected to tensile in-plane loading. The micro/macro-level approach was used for this study. The micro-level analysis used the 3-D unit cell model while macro-level analysis used the finite element analysis technique. A cross-ply laminate with double-edge notches was studied to investigate delamination, fiber splitting, and transverse matrix cracking in the structure. Numerical results were compared to previous experimental work.

THIS PAGE INTENTIONALLY LEFT BLANK

TABLE OF CONTENTS

I. INTRODUCTION

A. BACKGROUND

Throughout history technological development has been closely related to our ability to use and manipulate materials to suit our needs. Many modern composite materials offer design engineers desirable combinations of material properties unavailable in more traditional materials. Composites are often used as structural members because of their improved strength-to-weight ratio, stiffness-to-weight ratio, toughness, or corrosion resistance. They can also be engineered to provide a particular combination of properties by varying such factors as constituent materials, volume fraction of constituents, and fabrication/manufacturing processes. The primary drawback from most composites is their higher costs. However, increases in component costs are frequently offset by decreases in systemic costs due to weight savings.

B. PREVIOUS WORK

A number of investigations have been conducted concerning damage and failure in composite materials. In the first of their four paper series on Damage Mechanics of Composite Materials, Kortschot and Beaumont conducted an experimental study to establish a qualitative relationship between the notched strength and terminal damage state of double–edge-notched (DEN) cross-ply specimens. They also identified three primary failure modes for these specimens: fiber splits in the 0° plies, transverse ply matrix cracks in the 90° plies, and triangular delamination zones at the 0/90 interfaces. These modes are shown schematically in Figure 1. They also found that the angles at the

apex of the delamination zones measured between 5° and 10° for most specimens. [Ref. 1]

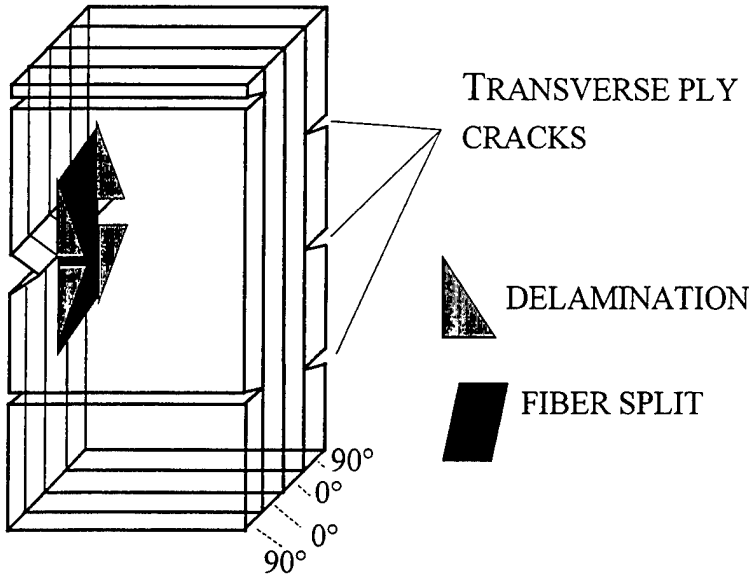

Figure 1 Failure Modes in a $(90/0)_s$ Laminate--After [Ref. 1]

The finite element method has been used by many investigators to model and predict the response of composite materials to various loads. Chen *et al* [Ref. 2] and Hitchings *et al* [Ref. 3] both approach the problem using fracture mechanics assumptions and strain energy release rate criteria for delamination propagation. Davidson *et al* [Ref. 4] simplified that approach further by employing a special crack-tip element in the expected damage region. Reedy *et al* [Ref. 5] modeled delamination by using an eight-noded hex constraint element to connect shell elements of different laminae. If their failure criterion was met, the connection was considered broken and delamination considered to have begun or grown.

Brewer and Lagace [Ref. 6] approached delamination from the viewpoint of the design engineer using known composite materials in structural applications. As such,

they sought a quick and efficient method for predicting delamination. They proposed and verified a Quadratic Delamination Criterion based on the interlaminar stresses calculated efficiently in Kassapoglou and Lagace's previous work [Ref. 7]. The primary advantage of their methods is computational simplicity; it enables the designer to predict delamination initiation without performing a complete finite element analysis of the structure.

Another approach to failure prediction using the finite element method involves using a micromechanical model to separately examine fiber and matrix stresses in composite laminae. Ardic *et al* [Ref. 8] conducted a study examining composites of dissimilar laminae using this methodology. Zhu *et al* [Ref. 9] developed their Direct Micromechanics Method (DMM) and compared it with phenomenological results for unidirectional composites.

C. OBJECTIVE

The objective of this study was to reproduce numerically damage patterns in DEN cross-ply continuous fiber composites that had been observed experimentally but which are still unexplained analytically. To achieve this a micro-/macromechanical model was applied in conjunction with appropriate failure criterion. A parametric study was then conducted to investigate the effects of notch size and specimen width on the delamination zone size.

II. SOLUTION METHODOLOGY

A. ANALYTIC

1. Determination of Material Properties

In order to effectively use composite materials, designers must be able to reliably determine their properties including their degradation as a result of damage. Structural analysis of composite components is conducted using one of two approaches: micro- or macromechanical. In macromechanical analysis, the component is treated as a pseudo-homogeneous body. The effective material properties of the pseudo-homogeneous body are either predicted through "smearing" or averaging the properties of its constituent materials, or they are determined experimentally. The smearing calculation is generally based on micromechanical analysis, but after the effective properties have been determined, there is no further need for the properties of the constituent materials.

Micromechanical analysis uses the properties of the constituent materials and their interaction to predict the response of the composite material. Three general approaches to micromechanical analysis are: the Rule of Mixtures (ROM), semi-empirical approaches, and methods of cells. Certain assumptions are common to each of these methods; for continuous fiber composites they include: homogeneous, linearly elastic, isotropic matrix material; perfect bonding between fiber and matrix; and regularly spaced, perfectly aligned, homogeneous fibers [Ref. 10].

The Rule of Mixtures is a rough tool for predicting composite properties through volume averaging; it is based on the strength of materials approach. Longitudinal properties result from the assumption that fibers and surrounding matrix material

experience the same strain. Transverse properties follow from the assumption that fiber and matrix are subjected to the same stress. Experimental work has shown that actual longitudinal properties of uniaxial laminae are comparable to those calculated through ROM; calculated transverse properties have proven to be less comparable. Thus, ROM is useful as a rule of thumb for estimating properties along the fiber orientation.

The semi-empirical approach is characterized by the Halpin-Tsai Equations which relate composite properties, p, to matrix properties, p_m, as follows:

$$\frac{p}{p_m} = \frac{1 + \xi \eta V_f}{1 - \eta V_f} \tag{1}$$

where the function η is of the form shown:

$$\eta = \frac{\frac{p_f}{p_m} - 1}{\frac{p_f}{p_m} + \xi} \tag{2}$$

and ξ is determined experimentally and depends on a variety of factors, including fiber volume fraction, fiber geometry, loading conditions, and which property, p, is sought. V_f is the volume fraction of the fiber. [Ref. 11]

The Rule of Mixtures and the Halpin-Tsai Equations provide means of determining smeared properties of a composite lamina in the linear elastic range. To progress beyond the linear elastic range into damage analysis and degradation of materials as a result of damage, another approach is required. The micromechanical method of cells was introduced by Aboudi [Ref. 12]; in it he assumed that a composite is a periodic array of matrix and reinforcement (fiber) materials. The analysis then

concentrates on a representative unit cell with displacement and traction continuity boundary conditions imposed at the interfaces. The unit cell is composed of four subcells, one consisting of reinforcement and three consisting of matrix material. Although it appears to imply that fibers have square cross-sections, because interfacial conditions are imposed on average vice point-wise bases, the geometry is not constrained. Pecknold [Ref 13] noted that Aboudi's model forms the basis for a finite element model and conducted an investigation of a simplified unit cell model. Kwon and his colleagues have refined the unit cell model to examine stresses in both fiber and matrix components at the micromechanical level [Ref. 14-20]. This model is particularly suitable for analyzing damage, for failure criteria can be applied to both fiber and matrix materials at the micromechanical level. This [Ref. 20], then, is the basis for this current work.

2. Micro-Macro Interaction

In this work, a combination of micro- and macro-mechanical approaches is used. Micro-mechanical analysis is used to determine smeared, effective composite properties. Finite element analysis uses the smeared properties in the constitutive equations to calculate macro- or elemental stresses and strains. These stresses and strains can then be used in a structural analysis or, as in this work, decomposed into micro- or subcell stresses and strains. Each subcell consists solely of fiber or matrix material, so failure criteria can then be applied to the microstresses and microstrains to determine failure initiation, progression, or mode. If failure is found to have occurred, the material properties of the constituent materials can then be degraded to reflect that and through the smearing process the degradation is carried through to the next iteration of the analysis.

Figure 2 illustrates the transitions and exchange of information between the two types of analysis.

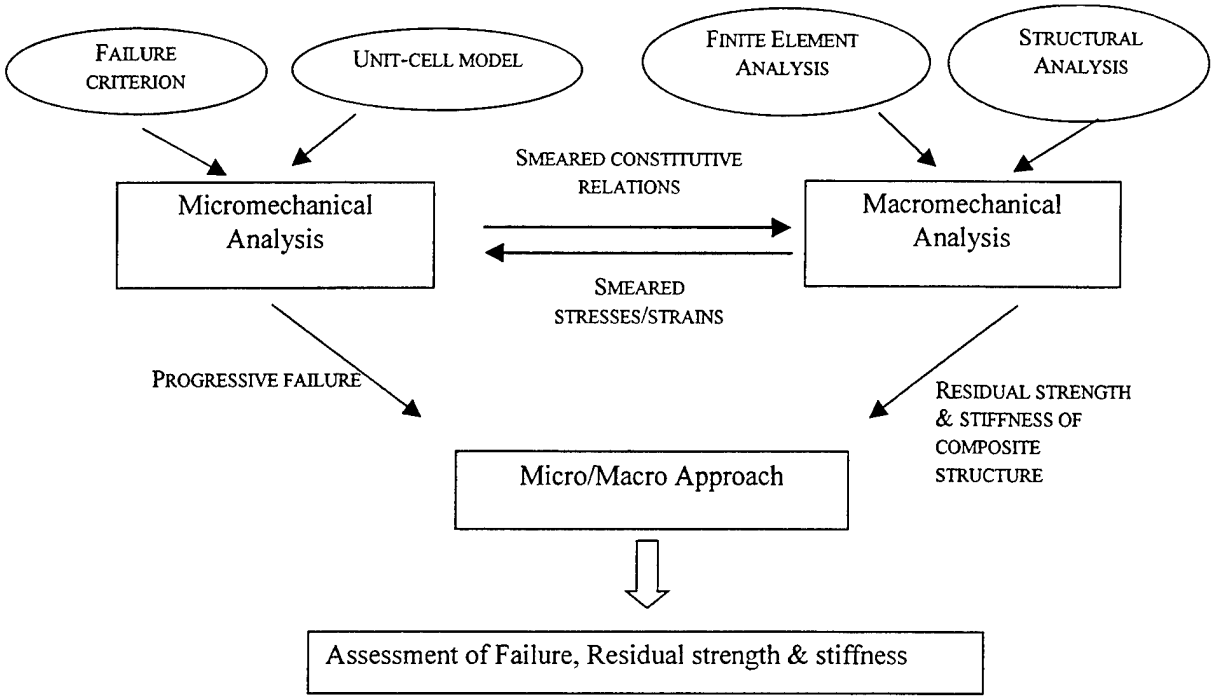

Figure 2 Micro/macromechanical Model

3. The Micromechanical Cell Model

Although micromechanical models for fibrous composites usually use only four subcells, eight subcells were used in this work because the computer code used was adapted from one developed for particulate composites which generally use an eight subcell model. The principles are the same, but the fiber occupies two subcells along its longitudinal direction. The unit cell is a three dimensional solid, rectangular, parallelepiped broken down into eight subcells, two containing fiber material and six containing matrix material. Taking advantage of symmetry only one quarter of the total cell is used; as shown in Figure 3.

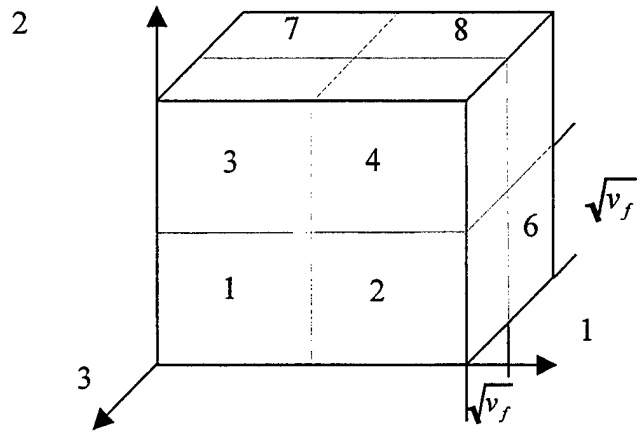

Figure 3 The Micromechanical Unit Cell

The size of each subcell is dependent on fiber volume fraction. The stresses and strains for each unit cell or element are the volume averaged subcell stresses and strains as shown in Equations (3) and (4)

$$\bar{\sigma}_{ij} = \frac{1}{2}\left[v_f\left(\sigma_{ij}^1 + \sigma_{ij}^2\right) + \sqrt{v_f}\left(1-\sqrt{v_f}\right)\left(\sigma_{ij}^3 + \sigma_{ij}^4 + \sigma_{ij}^5 + \sigma_{ij}^6\right) + \left(1-\sqrt{v_f}\right)^2\left(\sigma_{ij}^7 + \sigma_{ij}^8\right)\right] \quad (3)$$
$$i,j=1,3$$

$$\bar{\varepsilon}_{ij} = \frac{1}{2}\left[v_f\left(\varepsilon_{ij}^1 + \varepsilon_{ij}^2\right) + \sqrt{v_f}\left(1-\sqrt{v_f}\right)\left(\varepsilon_{ij}^3 + \varepsilon_{ij}^4 + \varepsilon_{ij}^5 + \varepsilon_{ij}^6\right) + \left(1-\sqrt{v_f}\right)^2\left(\varepsilon_{ij}^7 + \varepsilon_{ij}^8\right)\right] \quad (4)$$
$$i,j=1,3$$

where $\bar{\sigma}_{ij}$ and $\bar{\varepsilon}_{ij}$ are the elemental stresses and strains, σ_{ij}^k and ε_{ij}^k are subcell (k=1,8) stresses and strains, and v_f is the fiber volume fraction. Subcells 1 and 2 contain the fiber and subcells 3-8 contain matrix material. Stress continuity conditions at subcell interfaces are shown in Equation (5).

$$
\begin{aligned}
\sigma_{11}^{1} = \sigma_{11}^{2} \;,\; \sigma_{11}^{3} = \sigma_{11}^{4} \;,\; \sigma_{11}^{5} = \sigma_{11}^{6} \;,\; \sigma_{11}^{7} = \sigma_{11}^{8} \\
\sigma_{22}^{1} = \sigma_{22}^{3} \;,\; \sigma_{22}^{2} = \sigma_{22}^{4} \;,\; \sigma_{22}^{5} = \sigma_{22}^{7} \;,\; \sigma_{22}^{6} = \sigma_{22}^{8} \\
\sigma_{33}^{1} = \sigma_{33}^{5} \;,\; \sigma_{33}^{2} = \sigma_{33}^{6} \;,\; \sigma_{33}^{3} = \sigma_{33}^{7} \;,\; \sigma_{33}^{4} = \sigma_{33}^{8} \\
\sigma_{12}^{1} = \sigma_{12}^{2} \;,\; \sigma_{12}^{1} = \sigma_{12}^{3} \;,\; \sigma_{12}^{2} = \sigma_{12}^{4} \\
\sigma_{12}^{5} = \sigma_{12}^{6} \;,\; \sigma_{12}^{5} = \sigma_{12}^{7} \;,\; \sigma_{12}^{6} = \sigma_{12}^{8} \\
\sigma_{23}^{1} = \sigma_{23}^{3} \;,\; \sigma_{23}^{1} = \sigma_{23}^{5} \;,\; \sigma_{23}^{5} = \sigma_{23}^{7} \\
\sigma_{23}^{2} = \sigma_{23}^{4} \;,\; \sigma_{23}^{2} = \sigma_{23}^{6} \;,\; \sigma_{23}^{6} = \sigma_{23}^{8} \\
\sigma_{13}^{1} = \sigma_{13}^{2} \;,\; \sigma_{13}^{1} = \sigma_{13}^{5} \;,\; \sigma_{13}^{2} = \sigma_{13}^{6} \\
\sigma_{13}^{3} = \sigma_{13}^{4} \;,\; \sigma_{13}^{3} = \sigma_{13}^{7} \;,\; \sigma_{13}^{4} = \sigma_{13}^{8}
\end{aligned}
\tag{5}
$$

Individual subcells may experience different strains, but the sums of parallel longitudinal strains must be equal. A similar compatibility condition is imposed for transverse strains. Mathematically these conditions are shown in Equation (6):

$$
\begin{gathered}
\varepsilon_{11}^{1} + \varepsilon_{11}^{2} = \varepsilon_{11}^{3} + \varepsilon_{11}^{4} = \varepsilon_{11}^{5} + \varepsilon_{11}^{6} = \varepsilon_{11}^{7} + \varepsilon_{11}^{8} \\
\sqrt{v_f}\,\varepsilon_{22}^{1} + \left(1-\sqrt{v_f}\right)\varepsilon_{22}^{3} = \sqrt{v_f}\,\varepsilon_{22}^{2} + \left(1-\sqrt{v_f}\right)\varepsilon_{22}^{4} = \sqrt{v_f}\,\varepsilon_{22}^{5} + \left(1-\sqrt{v_f}\right)\varepsilon_{22}^{7} = \sqrt{v_f}\,\varepsilon_{22}^{6} + \left(1-\sqrt{v_f}\right)\varepsilon_{22}^{8} \\
\sqrt{v_f}\,\varepsilon_{33}^{1} + \left(1-\sqrt{v_f}\right)\varepsilon_{33}^{5} = \sqrt{v_f}\,\varepsilon_{33}^{2} + \left(1-\sqrt{v_f}\right)\varepsilon_{33}^{6} = \sqrt{v_f}\,\varepsilon_{33}^{3} + \left(1-\sqrt{v_f}\right)\varepsilon_{33}^{7} = \sqrt{v_f}\,\varepsilon_{33}^{4} + \left(1-\sqrt{v_f}\right)\varepsilon_{33}^{8}
\end{gathered}
\tag{6}
$$

Similar expressions are used for shear strain compatibility.

The constitutive equations for each subcell follow the form of the generalized Hooke's Law shown in Equation (7):

$$
\sigma_{ij}^{\alpha} = E_{ijkl}^{\alpha}\varepsilon_{kl}^{\alpha} \quad \mathrm{i,j,k,l} = 1,3 \text{ and } \alpha = 1,8 \tag{7}
$$

The assumption of perfect matrix/fiber bonding can be relaxed if the interface between fiber and matrix subcells is modeled using an equivalent spring as shown in Figure 4. This changes the strain compatibility equations to those of Equation (8).

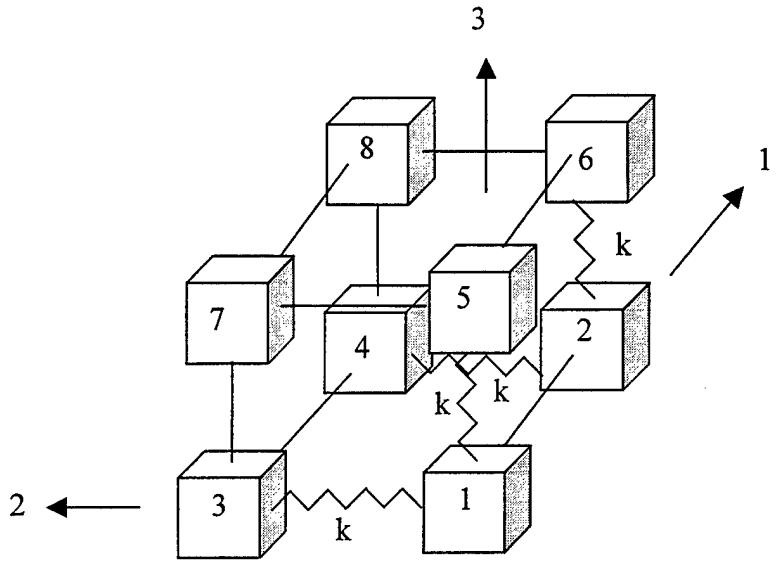

Figure 4 Micromechanical Unit Cell with Spring Interface

$$\varepsilon_{11}^{1}+\varepsilon_{11}^{2}=\varepsilon_{11}^{3}+\varepsilon_{11}^{4}=\varepsilon_{11}^{5}+\varepsilon_{11}^{6}=\varepsilon_{11}^{7}+\varepsilon_{11}^{8}$$

$$\left(\frac{E_{2222}^{1}}{k}+\sqrt{v_f}\right)\varepsilon_{22}^{1}+\left(1-\sqrt{v_f}\right)\varepsilon_{22}^{3}+\frac{E_{2211}^{1}}{k}\varepsilon_{11}^{1}+\frac{E_{2233}^{1}}{k}\varepsilon_{33}^{1}=\left(\frac{E_{2222}^{2}}{k}+\sqrt{v_f}\right)\varepsilon_{22}^{2}+\left(1-\sqrt{v_f}\right)\varepsilon_{22}^{4}+\frac{E_{2211}^{2}}{k}\varepsilon_{11}^{2}+\frac{E_{2233}^{2}}{k}\varepsilon_{33}^{2}$$

$$=\sqrt{v_f}\varepsilon_{22}^{5}+\left(1-\sqrt{v_f}\right)\varepsilon_{22}^{7}=\sqrt{v_f}\varepsilon_{22}^{6}+\left(1-\sqrt{v_f}\right)\varepsilon_{22}^{8} \qquad (8)$$

$$\left(\frac{E_{3333}^{1}}{k}+\sqrt{v_f}\right)\varepsilon_{33}^{1}+\left(1-\sqrt{v_f}\right)\varepsilon_{33}^{5}+\frac{E_{3311}^{1}}{k}\varepsilon_{11}^{1}+\frac{E_{3322}^{1}}{k}\varepsilon_{22}^{1}=\left(\frac{E_{3333}^{2}}{k}+\sqrt{v_f}\right)\varepsilon_{33}^{2}+\left(1-\sqrt{v_f}\right)\varepsilon_{33}^{6}+\frac{E_{3311}^{2}}{k}\varepsilon_{11}^{2}+\frac{E_{3322}^{2}}{k}\varepsilon_{22}^{2}$$

$$=\sqrt{v_f}\varepsilon_{33}^{3}+\left(1-\sqrt{v_f}\right)\varepsilon_{33}^{7}=\sqrt{v_f}\varepsilon_{33}^{4}+\left(1-\sqrt{v_f}\right)\varepsilon_{33}^{8}$$

Simultaneous solution of Equations (3) through (7) produces smeared composite material properties in terms of fiber and matrix material properties and their relative compositions. Combining this model with the Finite Element Method detailed in Section B, the following sequence of quantities can be calculated: elemental displacements → elemental strains → subcell strains → subcell stresses → elemental stresses.

In the study of progressive damage, therefore, failure criteria applied to fiber or matrix material at the micro-level will result in corresponding degradation of material properties at that level. This degradation will then be carried through subsequent iterations to reveal the failure processes of the composite.

B. NUMERICAL

1. Finite Element Method

The Finite Element Method of numerical analysis is used to solve the three dimensional elasticity problem: to determine stress and strain states of both fiber and matrix, and to apply failure criteria for each element. The finite element method converts a system of partial differential equations into a larger system of algebraic equations. It initially solves for nodal displacement and further processing calculates elemental strains. Application of the micromechanical model is used to determine subcell strains and stresses; these then serve as entering arguments for evaluating failure criteria for each element.

The derivation of the equations of equilibrium for a three dimensional solid in the absence of body forces can be found in any solid mechanics textbook [Ref 21]. Those equations are:

$$\frac{\partial \sigma_x}{\partial x}+\frac{\partial \tau_{xy}}{\partial y}+\frac{\partial \tau_{xz}}{\partial z}=0$$
$$\frac{\partial \sigma_y}{\partial y}+\frac{\partial \tau_{yx}}{\partial x}+\frac{\partial \tau_{yz}}{\partial z}=0 \qquad (9)$$
$$\frac{\partial \sigma_z}{\partial z}+\frac{\partial \tau_{zy}}{\partial y}+\frac{\partial \tau_{zx}}{\partial x}=0$$

At first glance there appear to be nine independent variables in these three equations; however, application of the moment equilibrium condition reduces this number to six:

$$\tau_{xy}=\tau_{yx}$$
$$\tau_{xz}=\tau_{zx} \qquad (10)$$
$$\tau_{yz}=\tau_{zy}$$

Below is the unit solid element illustrating the sign convention used with stress variables.

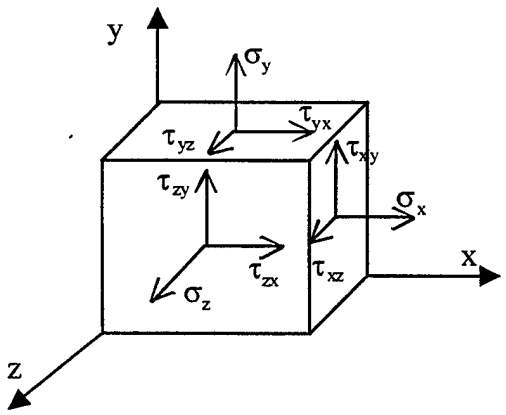

Figure 5 Sign Conventions

The variables 'u', 'v', and 'w' are used to represent displacements in the 'x', 'y', and 'z' directions, respectively. Assuming small displacements, strain is then defined as:

$$\varepsilon_x = \frac{\partial u}{\partial x};\ \varepsilon_y = \frac{\partial v}{\partial y};\ \varepsilon_z = \frac{\partial w}{\partial y}$$
$$\gamma_{xy} = \frac{\partial u}{\partial y} + \frac{\partial v}{\partial x};\ \gamma_{yz} = \frac{\partial w}{\partial y} + \frac{\partial v}{\partial z};\ \gamma_{xz} = \frac{\partial w}{\partial x} + \frac{\partial u}{\partial z} \tag{11}$$

These strain-displacement relationships can also be expressed in matrix form as shown in Equation (12):

$$\begin{Bmatrix} \varepsilon_x \\ \varepsilon_y \\ \varepsilon_z \\ \gamma_{xy} \\ \gamma_{yz} \\ \gamma_{zx} \end{Bmatrix} = \begin{bmatrix} \frac{\partial}{\partial x} & 0 & 0 \\ 0 & \frac{\partial}{\partial y} & 0 \\ 0 & 0 & \frac{\partial}{\partial z} \\ \frac{\partial}{\partial y} & \frac{\partial}{\partial x} & 0 \\ 0 & \frac{\partial}{\partial z} & \frac{\partial}{\partial y} \\ \frac{\partial}{\partial z} & 0 & \frac{\partial}{\partial x} \end{bmatrix} \begin{Bmatrix} u \\ v \\ w \end{Bmatrix} \tag{12}$$

The generalized Hooke's Law relating stress to strain can be expressed as:

$$\{\sigma\} = [D]\{\varepsilon\} \tag{13}$$

where $\{\sigma\}$ is the 6x1 stress column vector, $\{\varepsilon\}$ is the 6x1 strain vector and [D] is a 6x6 matrix of material properties. Thus Equations (9)-(13) combine as fifteen equations with fifteen unknowns, including several partial differential equations.

The derivation of the finite element equations from the three dimensional elasticity equations above is based on course notes and commonly available current

textbooks [Ref. 22]. The method of weighted residuals as modified by Galerkin is employed to develop the displacement based finite element equations. Eight noded isoparametric rectangular parallelepiped elements are used for the formulation. Linear shape functions are used for analytical and computational simplicity. Detailed derivation according to these precepts is continued below.

The first step in converting the partial differential equations into algebraic equations is to apply the method of weighted residuals to the three dimensional stress equilibrium Equations (9). To this end, each of the three equations of Equation (9) are multiplied by a weight function, W_i (i=1, 2, 3), which is continuous over the physical domain of the problem. Then, the three new product equations are integrated over the entire problem domain. The goal is to chose weight functions W_i which are orthogonal to the initial residuals of the equilibrium equations such that the integral of their product is zero. If 'V' is the domain volume of the problem, the weighted residual equations are shown in Equation (14):

$$
\begin{aligned}
I_1 &= \iiint_V \left(\frac{\partial \sigma_x}{\partial x} + \frac{\partial \tau_{xy}}{\partial y} + \frac{\partial \tau_{xz}}{\partial z} \right) W_1 dV = 0 \\
I_2 &= \iiint_V \left(\frac{\partial \tau_{xy}}{\partial x} + \frac{\partial \sigma_y}{\partial y} + \frac{\partial \tau_{yz}}{\partial z} \right) W_2 dV = 0 \\
I_3 &= \iiint_V \left(\frac{\partial \tau_{xz}}{\partial x} + \frac{\partial \tau_{yz}}{\partial y} + \frac{\partial \sigma_z}{\partial z} \right) W_3 dV = 0
\end{aligned}
\tag{14}
$$

At this point it should be noted that boundary conditions must be specified for Equation (9). The boundary conditions may be specified as either (a) essential or geometric boundary conditions in which some surface displacements are specified, (b) natural or

stress boundary conditions in which surface tractions are specified, or (c) a combination of these types of boundary conditions. Before applying boundary conditions, further manipulation of the weighted residuals is required as shown by Equation (15). Integration by parts will be performed in order to weaken the continuity requirements on the approximate solution.

$$
\begin{aligned}
I_1 &= \iiint_V \left[-\left(\sigma_x \frac{\partial W_1}{\partial x} + \tau_{xy} \frac{\partial W_1}{\partial y} + \tau_{xz} \frac{\partial W_1}{\partial z} \right) \right] dV + \iint_S \left(\sigma_x n_x W_1 + \tau_{xy} n_y W_1 + \tau_{xz} n_z W_1 \right) dS \\
I_2 &= \iiint_V \left[-\left(\tau_{xy} \frac{\partial W_2}{\partial x} + \sigma_y \frac{\partial W_2}{\partial y} + \tau_{yz} \frac{\partial W_2}{\partial z} \right) \right] dV + \iint_S \left(\tau_{xy} n_x W_2 + \sigma_y n_y W_2 + \tau_{yz} n_z W_2 \right) dS \\
I_3 &= \iiint_V \left[-\left(\tau_{xz} \frac{\partial W_3}{\partial x} + \tau_{yz} \frac{\partial W_3}{\partial y} + \sigma_z \frac{\partial W_3}{\partial z} \right) \right] dV + \iint_S \left(\tau_{xz} n_x W_3 + \tau_{yz} n_y W_3 + \sigma_z n_z W_3 \right) dS
\end{aligned}
\tag{15}
$$

In Equation (15) 'S' is the domain surface boundary, 'V' is the domain volume, and 'n_x', 'n_y', and 'n_z' are outward unit normal directional cosines in the 'x', 'y', and 'z' directions, respectively. The boundary stress conditions are defined by surface tractions as shown in Equation (16):

$$
\begin{aligned}
\phi_x &= \sigma_x n_x + \tau_{xy} n_y + \tau_{xz} n_z \\
\phi_y &= \tau_{xy} n_x + \sigma_y n_y + \tau_{yz} n_z \\
\phi_z &= \tau_{xz} n_x + \tau_{yz} n_y + \sigma_z n_z
\end{aligned}
\tag{16}
$$

Equations (15) and (16) can be combined and expressed in matrix form as:

$$\iiint_V \begin{Bmatrix} \sigma_x \dfrac{\partial W_1}{\partial x} + \tau_{xy} \dfrac{\partial W_1}{\partial y} + \tau_{xz} \dfrac{\partial W_1}{\partial z} \\ \tau_{xy} \dfrac{\partial W_2}{\partial x} + \sigma_y \dfrac{\partial W_2}{\partial y} + \tau_{yz} \dfrac{\partial W_2}{\partial z} \\ \tau_{xz} \dfrac{\partial W_3}{\partial x} + \tau_{yz} \dfrac{\partial W_3}{\partial y} + \sigma_z \dfrac{\partial W_3}{\partial z} \end{Bmatrix} dV = \iint_S \begin{Bmatrix} \phi_x n_x \\ \phi_y n_y \\ \phi_z n_z \end{Bmatrix} dS \tag{17}$$

Equation (17) can be further modified by separating the column vector inside the volume integral into the product of a 3x6 matrix and a 6x1 vector. This step, shown in Equation(18), isolates the weight function derivatives in the matrix from the stress terms in the vector.

$$\begin{Bmatrix} \sigma_x \dfrac{\partial W_1}{\partial x} + \tau_{xy} \dfrac{\partial W_1}{\partial y} + \tau_{xz} \dfrac{\partial W_1}{\partial z} \\ \tau_{xy} \dfrac{\partial W_2}{\partial x} + \sigma_y \dfrac{\partial W_2}{\partial y} + \tau_{yz} \dfrac{\partial W_2}{\partial z} \\ \tau_{xz} \dfrac{\partial W_3}{\partial x} + \tau_{yz} \dfrac{\partial W_3}{\partial y} + \sigma_z \dfrac{\partial W_3}{\partial z} \end{Bmatrix} = \begin{bmatrix} \dfrac{\partial W_1}{\partial x} & 0 & 0 & \dfrac{\partial W_1}{\partial y} & 0 & \dfrac{\partial W_1}{\partial z} \\ 0 & \dfrac{\partial W_2}{\partial y} & 0 & \dfrac{\partial W_2}{\partial x} & \dfrac{\partial W_2}{\partial z} & 0 \\ 0 & 0 & \dfrac{\partial W_3}{\partial z} & 0 & \dfrac{\partial W_3}{\partial y} & \dfrac{\partial W_3}{\partial x} \end{bmatrix} \begin{Bmatrix} \sigma_x \\ \sigma_y \\ \sigma_z \\ \tau_{xy} \\ \tau_{yz} \\ \tau_{xz} \end{Bmatrix} \tag{18}$$

Substitution of the strain-displacement relation of Equation (11) into the constitutive relations given by Equation (13) provides another useful identity as shown in Equation (19).

$$[D]\begin{Bmatrix} \frac{\partial u}{\partial x} \\ \frac{\partial v}{\partial y} \\ \frac{\partial w}{\partial z} \\ \frac{\partial u}{\partial y}+\frac{\partial v}{\partial x} \\ \frac{\partial v}{\partial z}+\frac{\partial w}{\partial y} \\ \frac{\partial w}{\partial x}+\frac{\partial u}{\partial z} \end{Bmatrix} = \begin{Bmatrix} \sigma_x \\ \sigma_y \\ \sigma_z \\ \tau_{xy} \\ \tau_{yz} \\ \tau_{xz} \end{Bmatrix} \tag{19}$$

Equation (12) is now substituted for the column vector on the left hand side of Equation (19). Equation (18) and the modified Equation (19) are substituted into Equation (17) to produce Equation (20).

$$\iiint_V \begin{bmatrix} \frac{\partial W_1}{\partial x} & 0 & 0 & \frac{\partial W_1}{\partial y} & 0 & \frac{\partial W_1}{\partial z} \\ 0 & \frac{\partial W_2}{\partial y} & 0 & \frac{\partial W_2}{\partial x} & \frac{\partial W_2}{\partial z} & 0 \\ 0 & 0 & \frac{\partial W_3}{\partial z} & 0 & \frac{\partial W_3}{\partial y} & \frac{\partial W_3}{\partial x} \end{bmatrix} [D] \begin{bmatrix} \frac{\partial}{\partial x} & 0 & 0 \\ 0 & \frac{\partial}{\partial y} & 0 \\ 0 & 0 & \frac{\partial}{\partial z} \\ \frac{\partial}{\partial y} & \frac{\partial}{\partial x} & 0 \\ 0 & \frac{\partial}{\partial z} & \frac{\partial}{\partial y} \\ \frac{\partial}{\partial z} & 0 & \frac{\partial}{\partial x} \end{bmatrix} \begin{Bmatrix} u \\ v \\ w \end{Bmatrix} dV = \iint_S \begin{Bmatrix} \phi_x n_x \\ \phi_y n_y \\ \phi_z n_z \end{Bmatrix} dS \tag{20}$$

The preceding manipulations of the elasticity relations have isolated displacement as the desired quantity. Now, to discretize the problem for an algebraic computational solution, assume that over a small domain each of the displacements can be represented by a polynomial. Discretization divides a three dimensional domain into small-but-finite

volume elements. In this formulation each finite element has eight nodes; each node can have three orthogonal displacements. Each element, therefore has a total of twenty-four degrees of freedom (dof). Calling 'u_i', 'v_i', and 'w_i' the displacements at each node, elemental displacements can be defined in terms of polynomial shape functions as follows:

$$u = \sum_{i=1}^{8} H_i u_i; \quad v = \sum_{i=1}^{8} H_i v_i; \quad w = \sum_{i=1}^{8} H_i w_i \tag{21}$$

The first partial derivatives of the shape functions exist as shown in Equations (22).

$$\begin{aligned}
&\frac{\partial u}{\partial x} = \sum_{i=1}^{8} \frac{\partial H_i}{\partial x} u_i; \quad \frac{\partial v}{\partial x} = \sum_{i=1}^{8} \frac{\partial H_i}{\partial x} v_i; \quad \frac{\partial w}{\partial x} = \sum_{i=1}^{8} \frac{\partial H_i}{\partial x} w_i; \\
&\frac{\partial u}{\partial y} = \sum_{i=1}^{8} \frac{\partial H_i}{\partial y} u_i; \quad \frac{\partial v}{\partial y} = \sum_{i=1}^{8} \frac{\partial H_i}{\partial y} v_i; \quad \frac{\partial w}{\partial y} = \sum_{i=1}^{8} \frac{\partial H_i}{\partial y} w_i; \\
&\frac{\partial u}{\partial z} = \sum_{i=1}^{8} \frac{\partial H_i}{\partial z} u_i; \quad \frac{\partial v}{\partial z} = \sum_{i=1}^{8} \frac{\partial H_i}{\partial z} v_i; \quad \frac{\partial w}{\partial z} = \sum_{i=1}^{8} \frac{\partial H_i}{\partial z} w_i;
\end{aligned} \tag{22}$$

The 3x1 elemental displacement vector can be expressed as the product of a 3x24 shape function matrix and a 24x1 nodal displacement vector. The product of the 6x3 partial differential matrix of Equation (20) and the 3x24 shape function matrix are typically combined into one 6x24 matrix. This matrix is referred to as the 'B' matrix in this formulation. In the shorthand notation shown in Equation (23), the 'B' matrix can be partitioned into sub-matrices, 'B_i', where i=1 to 8.

$$[B] = [[B_1][B_2][B_3][B_4][B_5][B_6][B_7][B_8]] \tag{23}$$

In this notation, the sub-matrices are defined in Equation (24).

$$[B_i]=\begin{bmatrix} \frac{\partial H_i}{\partial x} & 0 & 0 \\ 0 & \frac{\partial H_i}{\partial y} & 0 \\ 0 & 0 & \frac{\partial H_i}{\partial z} \\ \frac{\partial H_i}{\partial y} & \frac{\partial H_i}{\partial x} & 0 \\ 0 & \frac{\partial H_i}{\partial z} & \frac{\partial H_i}{\partial y} \\ \frac{\partial H_i}{\partial z} & 0 & \frac{\partial H_i}{\partial x} \end{bmatrix} \quad \text{where i = 1 to 8} \tag{24}$$

The Galerkin method takes the weighting functions as equivalent to the shape functions as shown in Equation (25).

$$W_1 = W_2 = W_3 = \begin{Bmatrix} H_1 \\ H_2 \\ H_3 \\ H_4 \\ H_5 \\ H_6 \\ H_7 \\ H_8 \end{Bmatrix} \tag{25}$$

The Galerkin method only requires that the weighting function be continuous over small discrete intervals which correspond to the sides of the finite elements. Based on the Galerkin weighting functions shown above, the weighting function matrix of Equation (20) can now be written in terms of the shape functions:

$$\begin{bmatrix} \frac{\partial W_1}{\partial x} & 0 & 0 & \frac{\partial W_1}{\partial y} & 0 & \frac{\partial W_1}{\partial z} \\ 0 & \frac{\partial W_2}{\partial y} & 0 & \frac{\partial W_2}{\partial x} & \frac{\partial W_2}{\partial z} & 0 \\ 0 & 0 & \frac{\partial W_3}{\partial z} & 0 & \frac{\partial W_3}{\partial y} & \frac{\partial W_3}{\partial x} \end{bmatrix} = [B]^T \tag{26}$$

Equation (26) can be incorporated in Equation (20) as follows:

$$\iiint_V [B]^T [D][B] dV \{d\} = \iint_S \begin{Bmatrix} \phi_x \{H_i\} \\ \phi_y \{H_i\} \\ \phi_z \{H_i\} \end{Bmatrix} dS \tag{27}$$

In Equation (27), {d} is the displacement vector which has grown from the 3x1 vector of 'u', 'v', and 'w' to a 24x1 vector of the nodal displacements 'u_i', 'v_i', and 'w_i'. The 3x1 vector in the surface integral on the right-hand side has an 8x1 vector in each term so that the entire integrand is shorthand for a 24x1 vector of discretized surface boundary tractions. The original three equilibrium elasticity partial differential equations have now been transformed to a matrix equation in 24 terms for each solid element. The integrals in Equation (27) may be easily solved if simple shape functions are chosen and if the modeled geometry is relatively simple.

If the modeled geometry is complex, the finite element geometry can be simplified by use of a transformation mapping to another reference space. In order to map 'x', 'y', and 'z' coordinates of an irregularly shaped element onto 'r', 's', and 't' coordinates for a rectangular parallelepiped, a Jacobian transformation matrix is required. The Jacobian transform matrix scales each component of the original space to a new space. Equation (28) shows the Jacobian for an 'xyz' system mapped to an 'rst' system:

$$[J]=\begin{bmatrix} \frac{\partial x}{\partial r} & \frac{\partial y}{\partial r} & \frac{\partial z}{\partial r} \\ \frac{\partial x}{\partial s} & \frac{\partial y}{\partial s} & \frac{\partial z}{\partial s} \\ \frac{\partial x}{\partial t} & \frac{\partial y}{\partial t} & \frac{\partial z}{\partial t} \end{bmatrix} \tag{28}$$

In terms of the shape functions and nodal points the Jacobian is shown in Equation (29).

$$[J]=\begin{bmatrix} \sum_{i=1}^{8}\frac{\partial H_i}{\partial r}x_i & \sum_{i=1}^{8}\frac{\partial H_i}{\partial r}y_i & \sum_{i=1}^{8}\frac{\partial H_i}{\partial r}z_i \\ \sum_{i=1}^{8}\frac{\partial H_i}{\partial s}x_i & \sum_{i=1}^{8}\frac{\partial H_i}{\partial s}y_i & \sum_{i=1}^{8}\frac{\partial H_i}{\partial s}z_i \\ \sum_{i=1}^{8}\frac{\partial H_i}{\partial t}x_i & \sum_{i=1}^{8}\frac{\partial H_i}{\partial t}y_i & \sum_{i=1}^{8}\frac{\partial H_i}{\partial t}z_i \end{bmatrix} \tag{29}$$

Since the finite element integral equation includes the partial derivatives of the shape functions with respect to the 'xyz' coordinate system, the inverse of the Jacobian is required. Let $[J]^{-1}=[\Gamma]$, where $[\Gamma]$ is a 3x3 matrix. The shape function derivatives with respect to the 'xyz' system are now expressed in Equation (30) with respect to the 'rst' system.

$$\begin{aligned} \frac{\partial H_i}{\partial x} &= \Gamma_{11}\frac{\partial H_i}{\partial r}+\Gamma_{12}\frac{\partial H_i}{\partial s}+\Gamma_{13}\frac{\partial H_i}{\partial t} \\ \frac{\partial H_i}{\partial y} &= \Gamma_{21}\frac{\partial H_i}{\partial r}+\Gamma_{22}\frac{\partial H_i}{\partial s}+\Gamma_{23}\frac{\partial H_i}{\partial t} \quad \text{i = 1 to 8} \\ \frac{\partial H_i}{\partial z} &= \Gamma_{31}\frac{\partial H_i}{\partial r}+\Gamma_{32}\frac{\partial H_i}{\partial s}+\Gamma_{33}\frac{\partial H_i}{\partial t} \end{aligned} \tag{30}$$

Equation (30) is used to calculate the [B] and $[B]^T$ matrices in the 'rst' system. Equation (29) is used to transform the volume differential. Application of these transformations to the left-hand side of Equation (27) is shown in Equation (31).

$$\iiint_V [B]^T [D][B] dV(x,y,z)\{d\} = \iiint_V [B]^T [D][B]|J| dV(r,s,t)\{d\} \tag{31}$$

The transformation to the 'rst' coordinate system results in simplified finite element integrals. The resultant transformed elements are termed isoparametric elements. The term isoparametric refers to the equality between the degree of the equations for transforming 'xyz' into 'rst' coordinates and the degree of the shape functions for estimating displacement. The shape functions in the 'rst' system are shown in Equation (32).

$$\begin{aligned}
H_1 &= \tfrac{1}{4}(1+r)(1+s)(1+t) \\
H_2 &= \tfrac{1}{4}(1+r)(1-s)(1+t) \\
H_3 &= \tfrac{1}{4}(1+r)(1-s)(1-t) \\
H_4 &= \tfrac{1}{4}(1+r)(1+s)(1-t) \\
H_5 &= \tfrac{1}{4}(1-r)(1+s)(1+t) \\
H_6 &= \tfrac{1}{4}(1-r)(1-s)(1+t) \\
H_7 &= \tfrac{1}{4}(1-r)(1-s)(1-t) \\
H_8 &= \tfrac{1}{4}(1-r)(1+s)(1-t)
\end{aligned} \tag{32}$$

Gauss Quadrature is used to numerically calculate the integrals. The volume integral is redefined as the triple summation from 1 to the number of integration points (NIP) of the integrand evaluated at Gauss integration points (r_i, s_i, and t_i) multiplied by weight factors as shown in Equation (33).

$$\iiint_V [B]^T [D][B] J \, dV(r,s,t)\{d\} = \sum_{i=1}^{NIP}\sum_{j=1}^{NIP}\sum_{k=1}^{NIP} [B]^T [D][B] J W_i W_j W_k \{d\} \tag{33}$$

The results of the numerical integration may vary over the elements in the domain of the model. Each of these results can be expressed as a 24x24 elemental stiffness matrix, $[K_e]$.

Recall the surface traction boundary conditions from the right-hand side of Equation (20). The integration of the directional component of the applied stress over the element surface area to which the stress is applied is equal to the external force applied to the element. The result of the integration is a 24x1 vector $\{F_e\}$ which is equivalent to the force in the 'x', 'y', and 'z' direction applied to a surface of the solid. Substituting these resultant terms into Equation (20) completes the finite element derivation shown in Equation (34).

$$[K_e]\{d\} = \{F_e\} \tag{34}$$

The finite element method involves combining these elemental matrix equations with given boundary conditions to form a large system of simultaneous equations to be solved numerically.

2. Implementation

The actual finite element analysis for this study was conducted using a FORTRAN driver for three-dimensional static analysis based in large part on the subroutines developed by Akin [Ref. 23]. Pre- and post-processing were conducted using various MATLAB programs.

The preprocessor generated an appropriately formatted text file containing material properties, nodal coordinates, element connectivity, boundary conditions, and loading data.

The FORTRAN program used several subroutines to read the input data and store it semi-dynamically. All data was stored in one of two massive arrays, one for integers and one for floating point variables, and pseudo-pointers were used to track the location of the first element of each matrix of interest. The memory allocation for these two arrays was calculated based upon the input data. After the input and housekeeping subroutines were completed, the heart of the analysis was controlled by subroutine FEMST. It called subroutine EL3D8A to calculate elemental stiffness matrices and assemble them into the system stiffness matrix. The stiffness matrices were calculated using the micromechanical model and Gauss Quadrature with two integration points in each coordinate direction for a total of eight integration points per element. Subroutine MA3D6F calculated material property matrices for composite elements, including transforming those matrices to account for fiber orientation. After the system matrix was assembled, boundary conditions were applied, and Equation (34) was solved for the nodal displacements using subroutines FACTOR and SOLVE. FACTOR uses the Cholesky method to factor the square system stiffness matrix into the product of a lower triangular matrix and its transpose. SOLVE uses Cholesky-Gauss methods of forward and back substitutions to complete the solution.

In the process of calculating the residual, elemental stresses and strains are calculated and then decomposed into subcell stresses and strains. These values can then

be used to evaluate matrix and fiber failure criterion and degrade the appropriate corresponding material properties if necessary.

The FORTRAN program writes its output to five main files: OUTPUT, DISPL, MATSTS, FIBSTS, and STRESS. OUTPUT is essentially an echo of the input file; DISPL is the u, v, and w displacements of each node; MATSTS contains the matrix subcell stresses at each integration point; FIBSTS contains the fiber subcell stresses at each integration point; and STRESS contains the complete stress state of each element. These data files were then read into various MATLAB programs for further analysis and visualization.

C. FAILURE CRITERION

The nature of the failure modes being investigated in this study, delamination and splitting, dictates that matrix material behavior be of primary interest. These phenomena are of interest because they can cause a structure to fail at much lower than expected loads. Delamination is an inter-laminar process; as such, the inter-laminar, through-thickness, or z-direction stresses are expected to be the controlling factor in its initiation. Brewer and Lagace [Ref. 6] proposed the following criterion for delamination:

$$\left(\frac{\sigma_z^t}{Z^t}\right)^2 + \left(\frac{\sigma_z^c}{Z^c}\right)^2 + \left(\frac{\tau_{xz}}{Z^s}\right)^2 + \left(\frac{\tau_{yz}}{Z^s}\right)^2 \geq 1 \tag{35}$$

Where Z^s is the shear strength, Z^t and Z^c are normal strengths in tension and compression, respectively; and τ_{xz} and τ_{yz} are interlaminar shear stresses, σ^t is interlaminar tensile stress, and σ^c is interlaminar compressive stress. This criterion will be the starting point of this investigation in which the failure criterion will be applied to generate a delamination zone similar to that observed experimentally. Assuming that the

isotropic matrix material is twice as strong in tension as it is in shear and four times as strong in compression as it is in tension, Equation (35) can be rearranged in terms of a single strength value as shown in Equation (36):

$$\left(\sigma_z{}^{t}\right)^2 + \left(\frac{\sigma_z{}^{c}}{4}\right)^2 + 4\left(\tau_{xz}^2 + \tau_{yz}^2\right) \geq \left(Z^t\right)^2 \tag{36}$$

In this form, this criterion can be evaluated without necessarily knowing the strength of the material in question. A stress profile calculated from the left-hand side of Equation (36) can be plotted and used to evaluate the suitability of the criterion.

Similar criterion was applied using stresses transverse to the fiber direction to evaluate fiber splitting and transverse cracking.

III. RESULTS AND DISCUSSION

A. COMPARISON OF 2-LAYER MODEL TO 3-LAYER MODEL TO EXPERIMENTAL RESULTS

In their experimental work Kortschot and Beaumont [Ref. 1] applied tensile loading to double-edge-notched graphite-epoxy specimens of various cross-ply lay-ups and sizes. They observed that delamination along the 0/90 interfaces progressed from the notch tip in a triangular zone upward and toward the center of the specimen. As the splits in 0° plies grew, the aspect ratio of the delamination triangle remained constant. The measured angles at the apex of each specimen's delamination triangle were found to consistently remain between 5° and 10°.

In this study two models were used to simulate the behavior observed by Kortschot and Beaumont. A two-layer model consisting of two laminae, one with fibers oriented along the direction of loading (0°) and one with fibers oriented transverse to the loading direction (90°), was compared with a three-layer model consisting of the same two laminae plus a thin "delamination layer" consisting solely of isotropic matrix material inserted between the two laminae. The same material properties and geometry were used for each model. The material properties of the two laminae of each model differed only by their orientation. The properties of the constituents of the specific composite used in the experimental work were unavailable, but values were chosen so that they were within approximate ranges for graphite fibers and epoxy matrix and that their smeared values were comparable to those cited by those investigators; the values used are shown in Table 1. The lay-up modeled was $(90/0)_s$, that is, two 0° plies sandwiched between a pair of 90° plies. Geometric and laminar symmetry conditions

allowed for a proper model of the specimens using only one-eighth of the original. Planes of symmetry were the mid-plane both longitudinally and transversely and the plane between the 0° plies. Nodes located on these planes were constrained in the direction(s) normal to their respective planes of symmetry. As in the experimental work, the modeled notch angle was 60°.

Table 1 Lamina Dimensions and Material Properties

Width	5mm
Length	10mm
Thickness	1.5mm
Notch Length/Specimen Width (2a/w)	0.125
Fiber Longitudinal Young's Modulus (E_{fl})	202.5 GPa
Matrix Young's Modulus (E_m)	3.45 GPa
Fiber Transverse Young's Modulus (E_{ft})	15.75 GPa
Fiber Poisson Ratio (12 direction)	0.29
Fiber Poisson Ratio (23 direction)	0.25
Matrix Poisson Ratio	0.35
Fiber Shear Modulus (12 direction)	15.75 GPa
Volume Fraction	0.66

To evaluate the suitability of the two-layer model, the left-hand side of Equation (36) was applied to the volume averaged matrix subcell stresses for each element in the 0° lamina. This profile is shown for the entire modeled section in Figure 6 and for the refined mesh area in Figure 7.

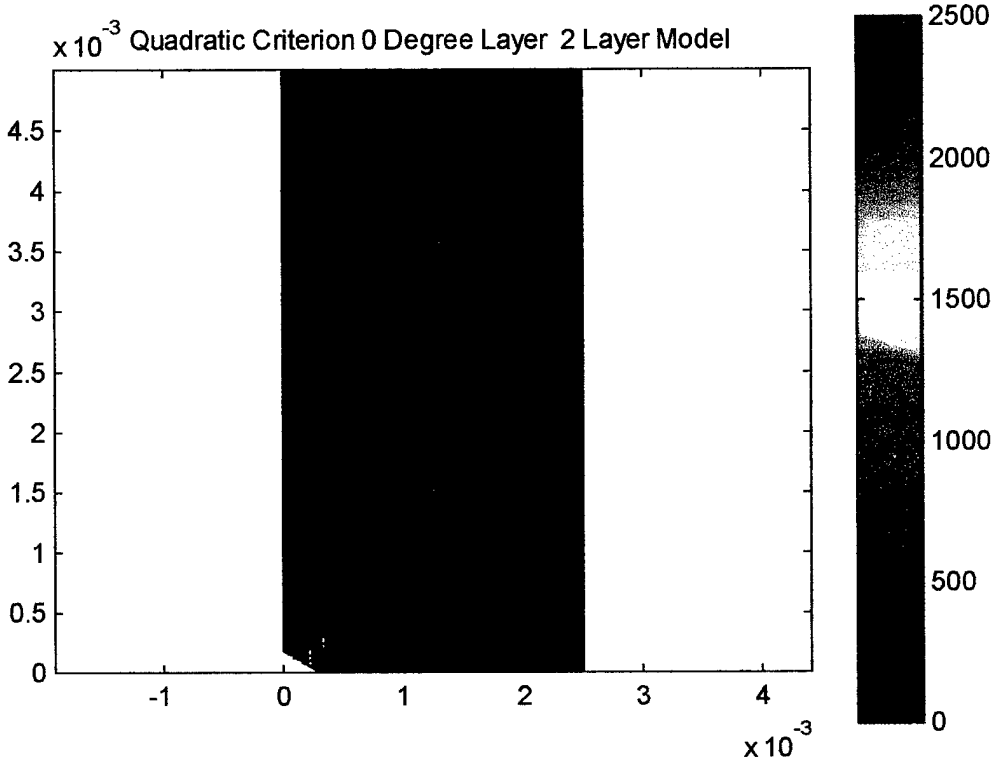

Figure 6 Delamination Zone 0° Ply 2 Layer Model

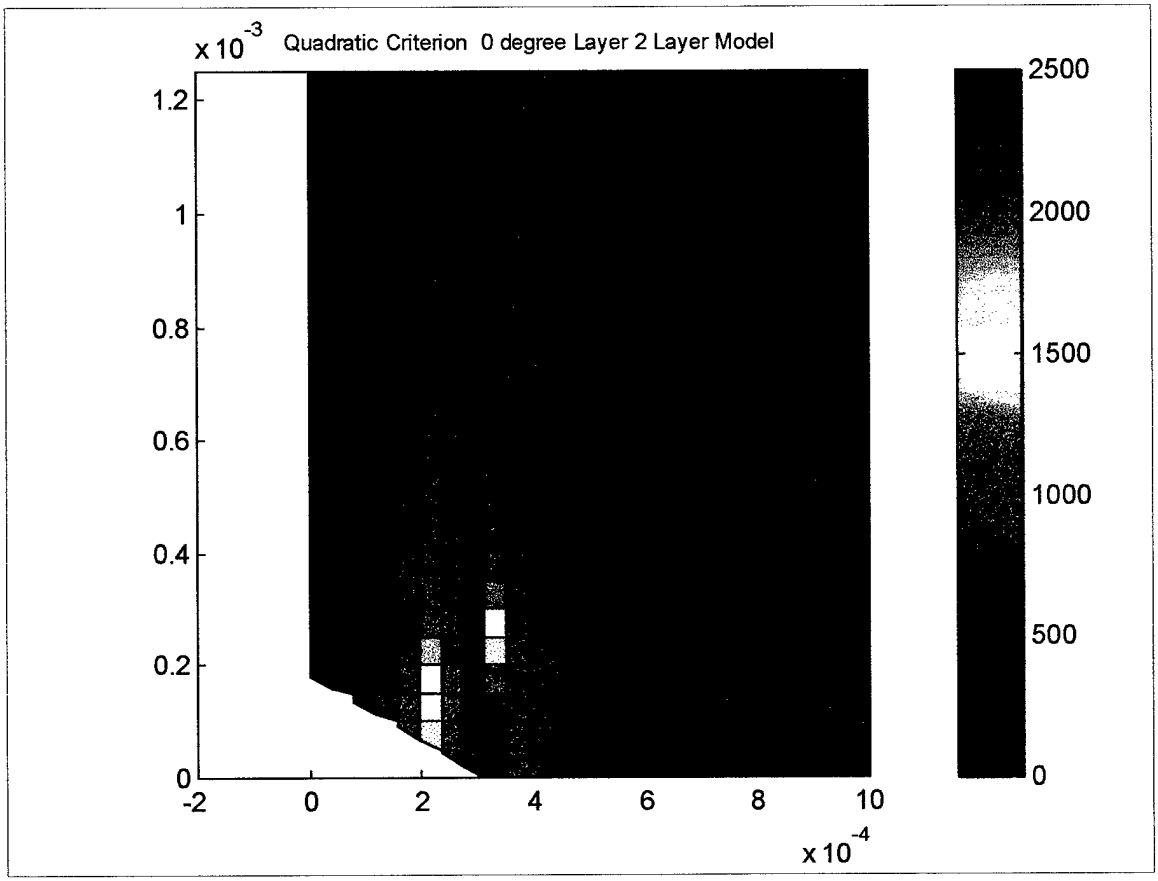

Figure 7 Delamination Zone 0° Ply 2 Layer Model

The same sort of profile was generated for the three layer model based on the stress states of the elements in the delamination layer. These are shown in Figure 8 and Figure 9.

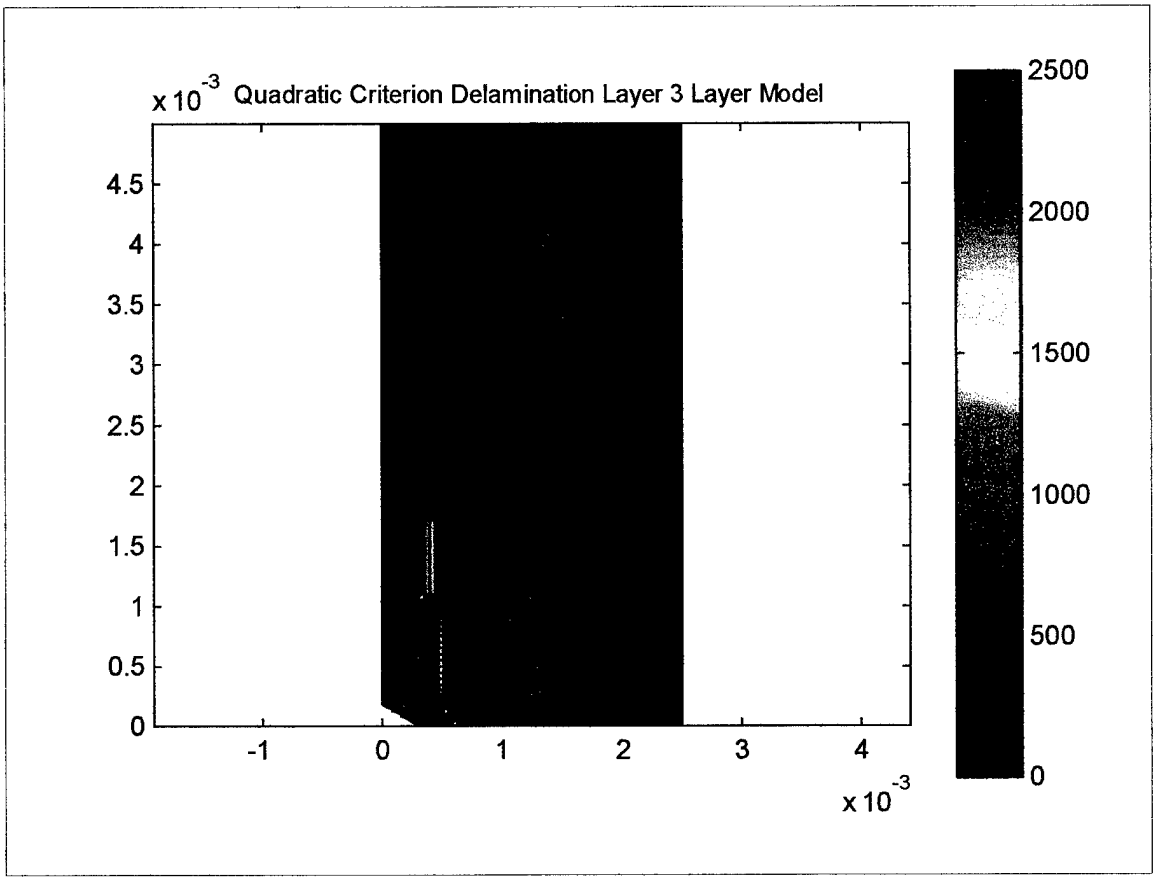

Figure 8 Delamination Zone 3 Layer Model

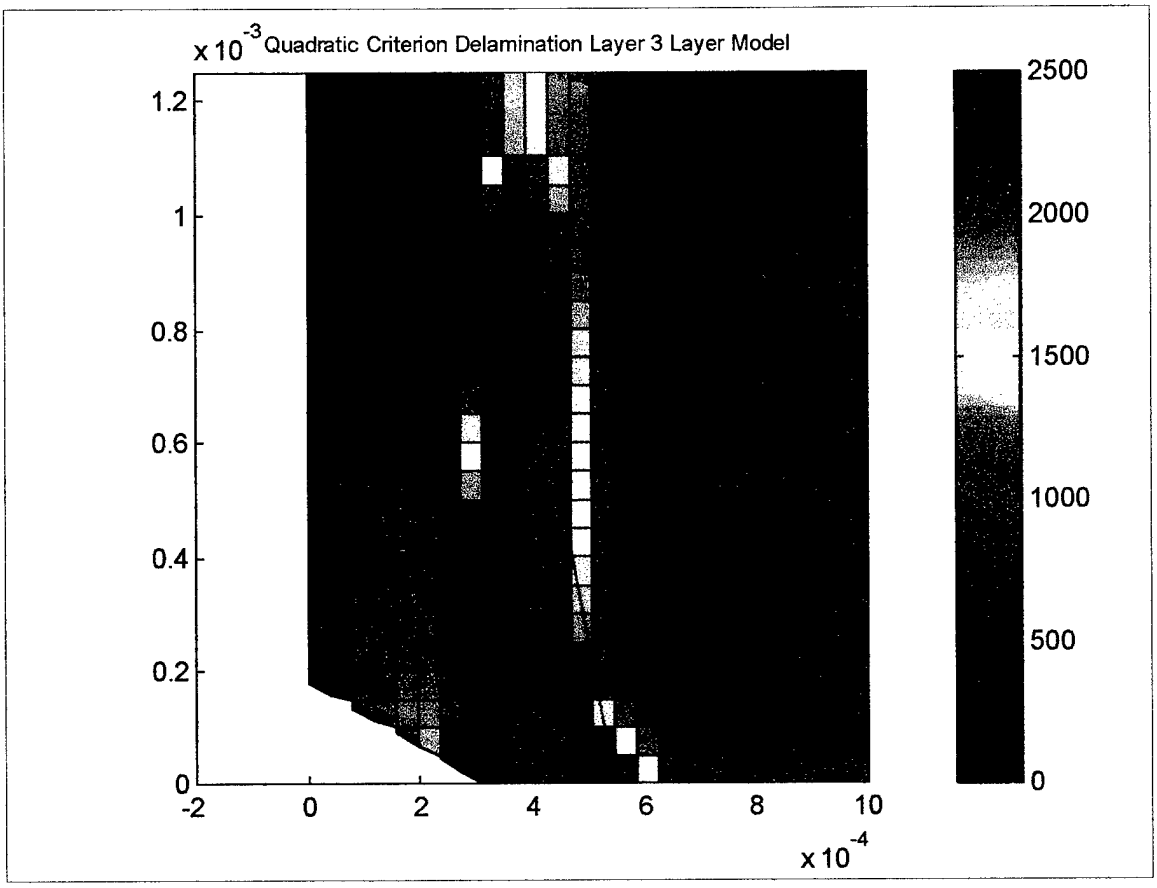

Figure 9 Delamination Zone 3 Layer Model

It is apparent from Figures 6-9 that the three-layer model more closely resembles the delamination zone observed experimentally. The apex angle of the delamination triangle (superimposed in Figure 9) in the three layer model is approximately 10°, comparing favorably with experimental observations. While the two layer model's stress profile does not have the characteristic triangular shape of a delamination region, a similar profile generated from its transverse matrix subcell stresses does compare favorably with observed 0° ply splitting. This profile is shown in Figures 10 and 11.

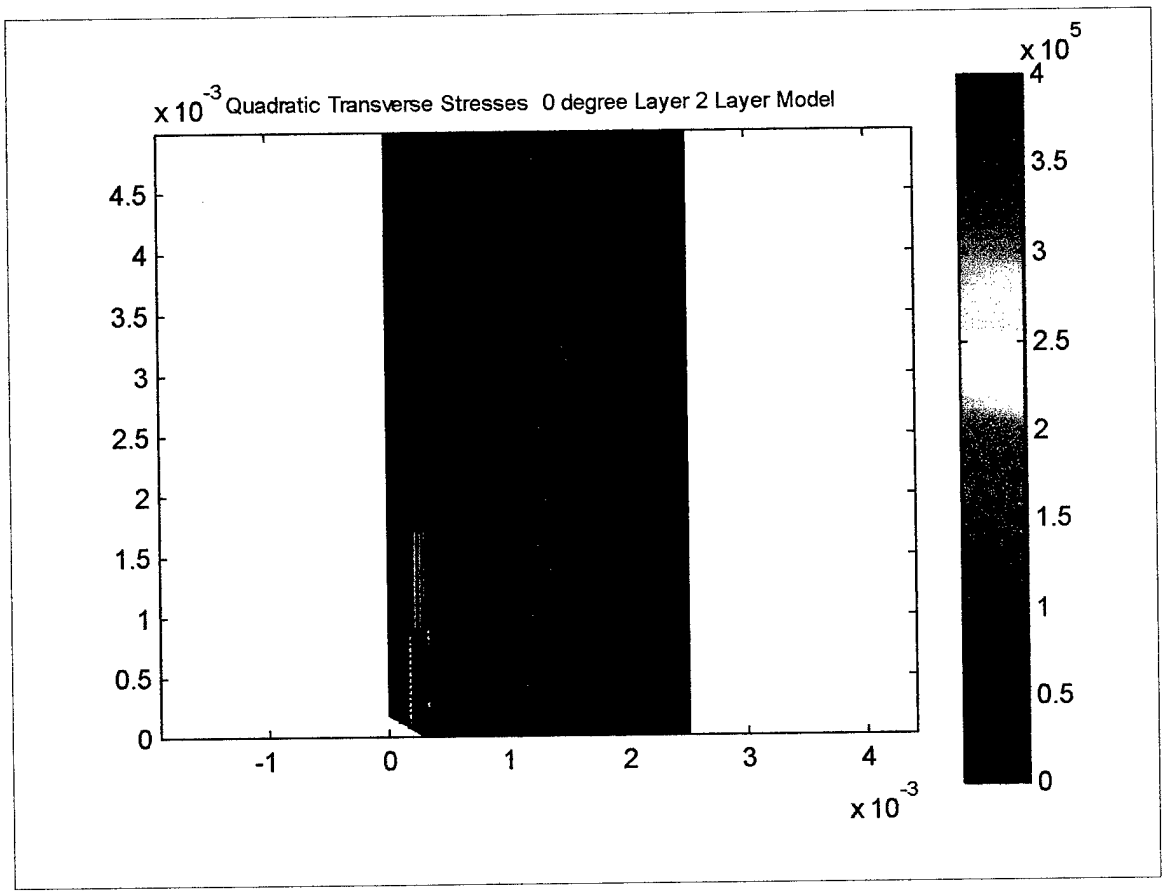

Figure 10 Fiber Splitting in 0° Ply, 2 Layer Model

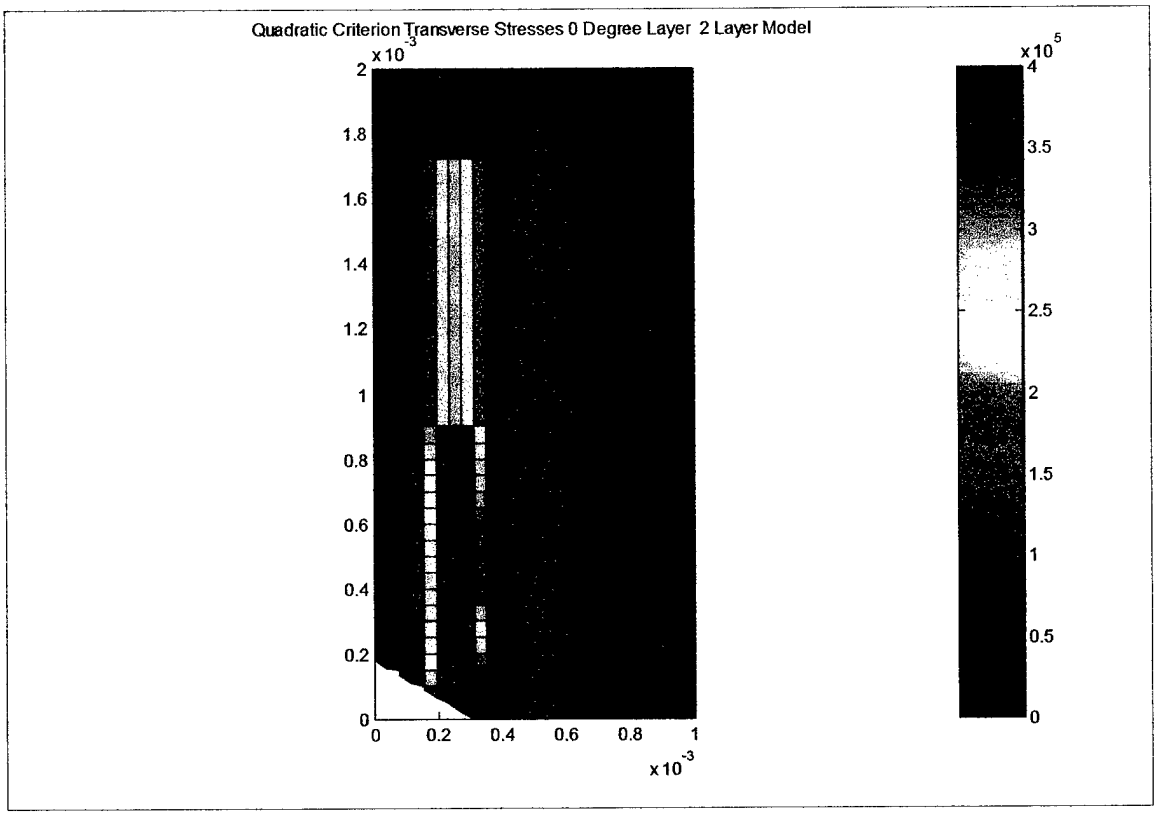

Figure 11 Fiber Splitting in 0° Ply, 2 Layer Model

The three layer model not only displays a more realistic delamination zone, the transverse stress profiles in the 0° and 90° laminae also reflect fiber splitting and transverse cracking, respectively. As observed experimentally and expected with graphite fibers, transverse cracking permeates the 90° lamina. These effects are illustrated in Figures 12-14.

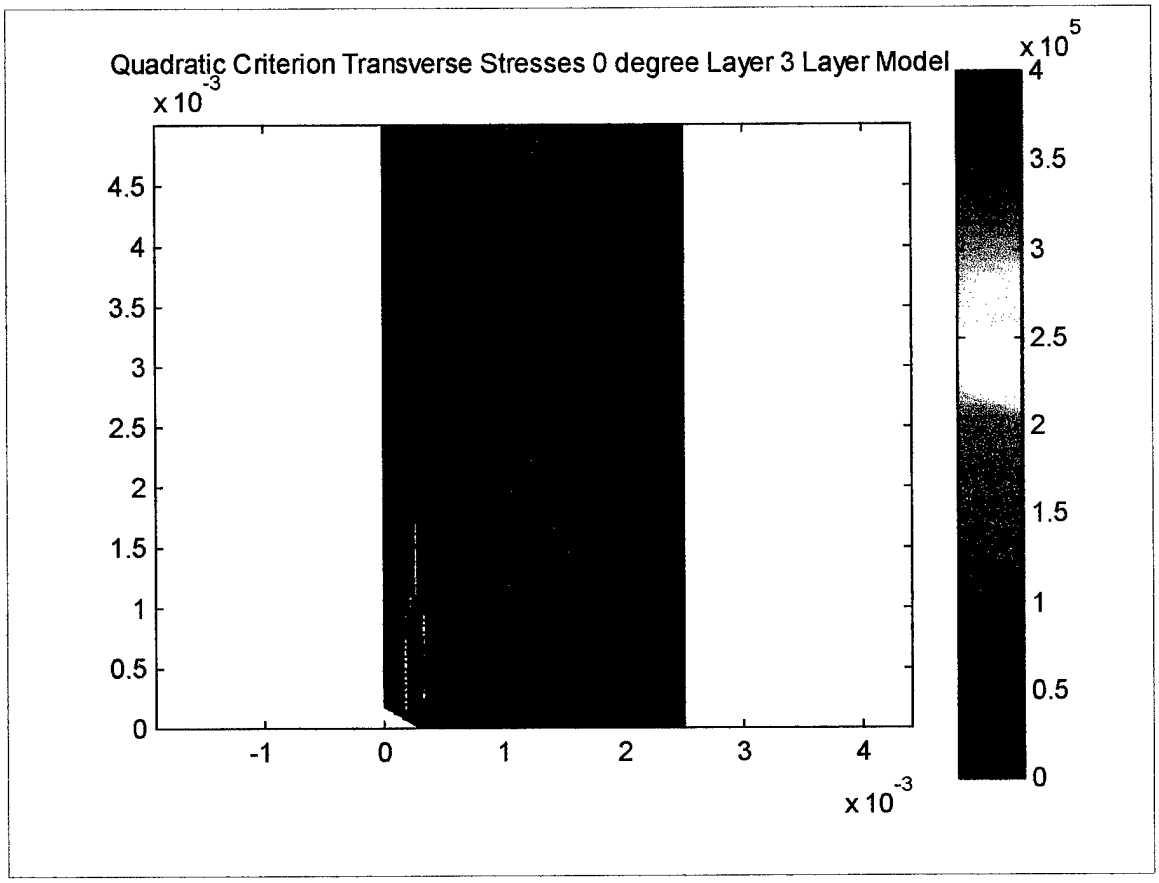

Figure 12 Fiber Splitting in 0° Ply, 3 Layer Model

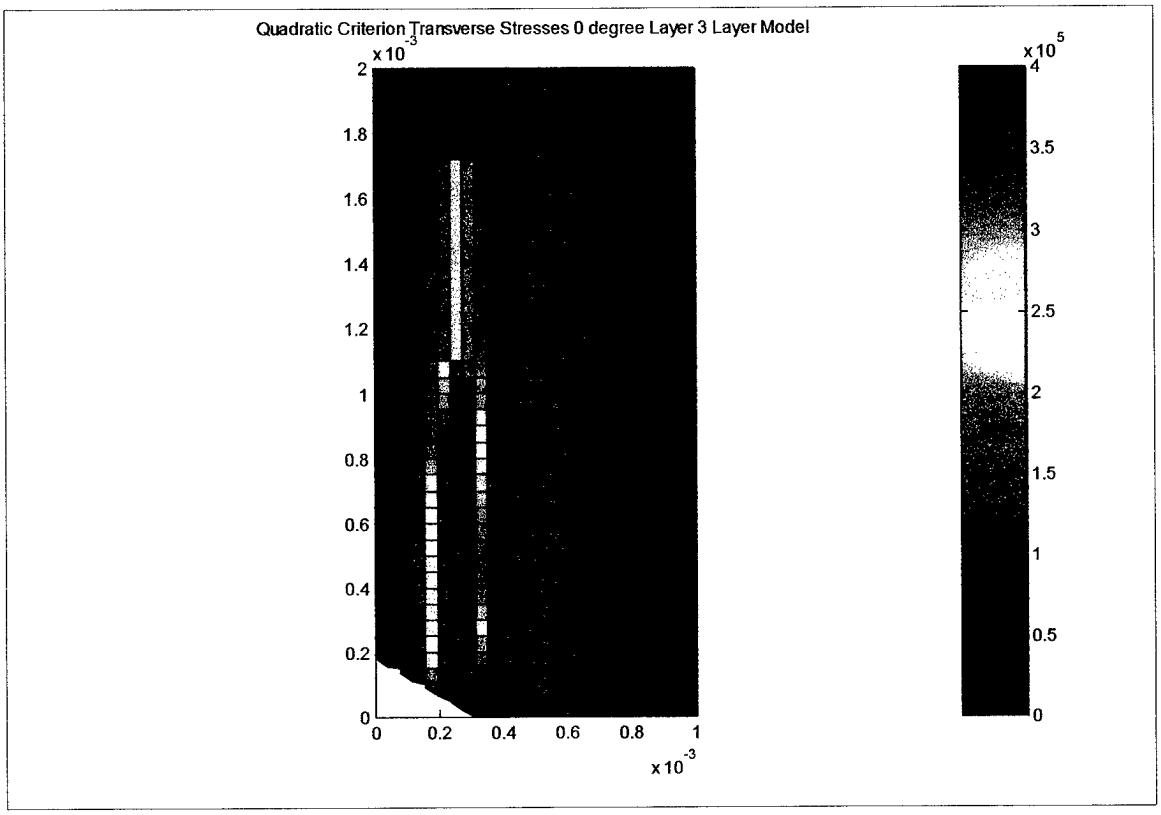

Figure 13 Fiber Splitting in 0° Ply, 3 Layer Model

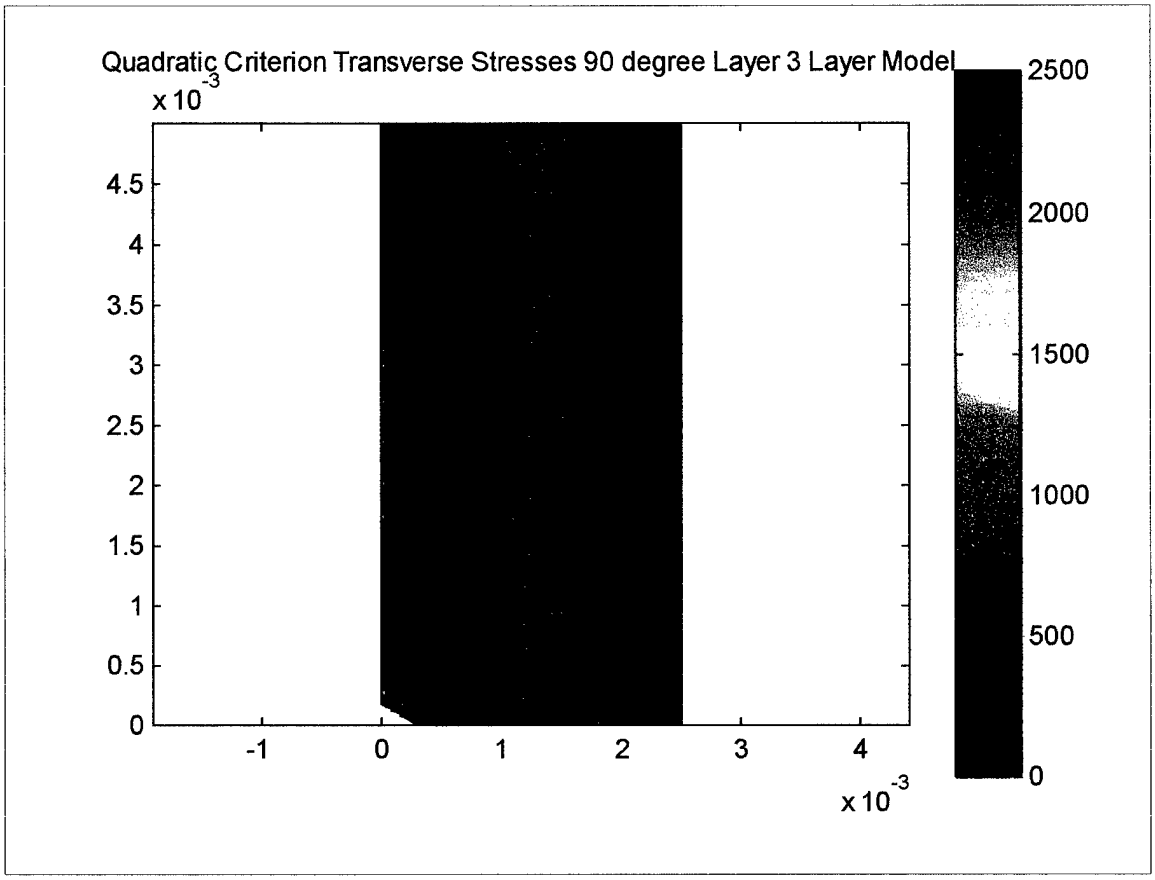

Figure 14 Transverse Cracking 90° Ply, 3 Layer Model

B. PARAMETRIC STUDY

A parametric study varying notch length and specimen width was conducted to further evaluate the quadratic delamination criterion as applied to the three layer model. Using the original crack length to width ratio (2a/w=0.125), samples 5, 10, 20, and 40 mm wide were simulated. The resulting delamination zones are shown in Figures 15-18. The apex angles of those zones ranged from 6°-12°.

In the pre-processor used, the nodes were placed as a function of crack length and specimen width and length; as such, each of these different specimens has the same number of elements. Therefore, the wider specimens have larger elements and some detail is lost. Nevertheless, the influence of the fiber splits and the general triangular shape of the delamination zones can be seen.

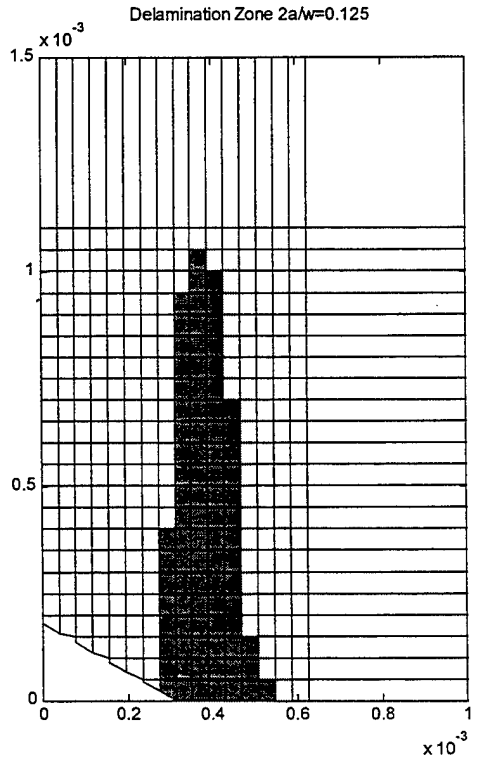

Figure 15 Delamination Zone w=5mm

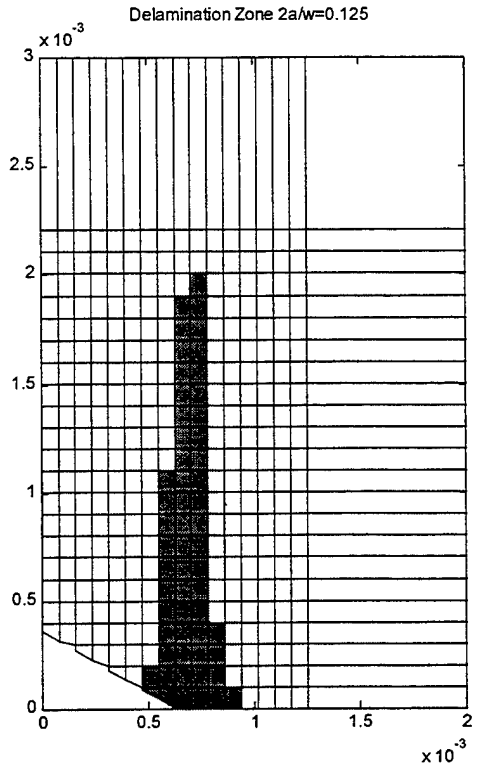

Figure 16 Delamination Zone w=10mm

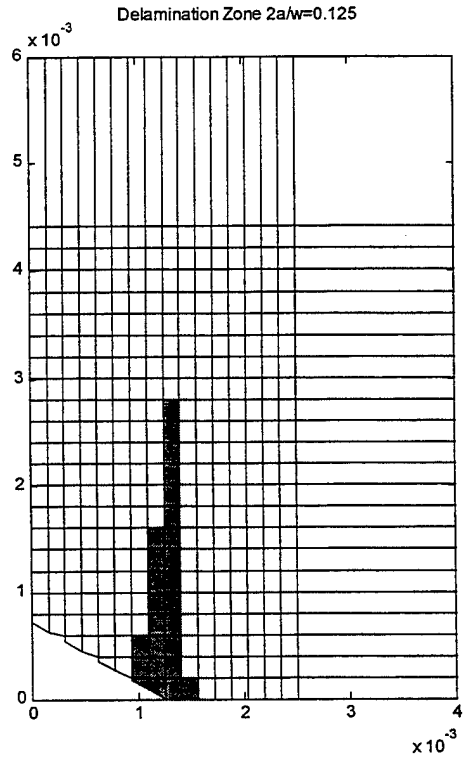

Figure 17 Delamination Zone w=20mm

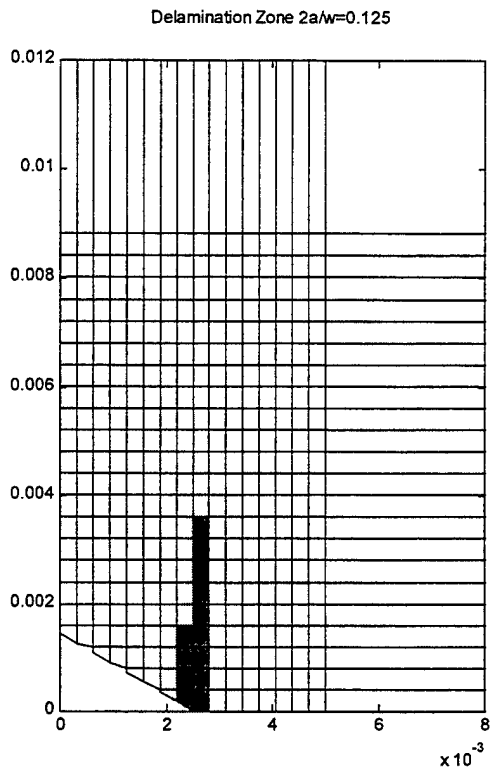

Figure 18 Delamination Zone w=40mm

For the same four widths crack length to width ratio was also varied. Figures 19-22 show delamination zones for those specimens. For the first three of these specimens apex angles range from 6°-13°. Once again the mesh effects appear to suggest that delamination is a size-dependent phenomenon. This coarsening is most apparent in the 40mm specimen, Figure 22.

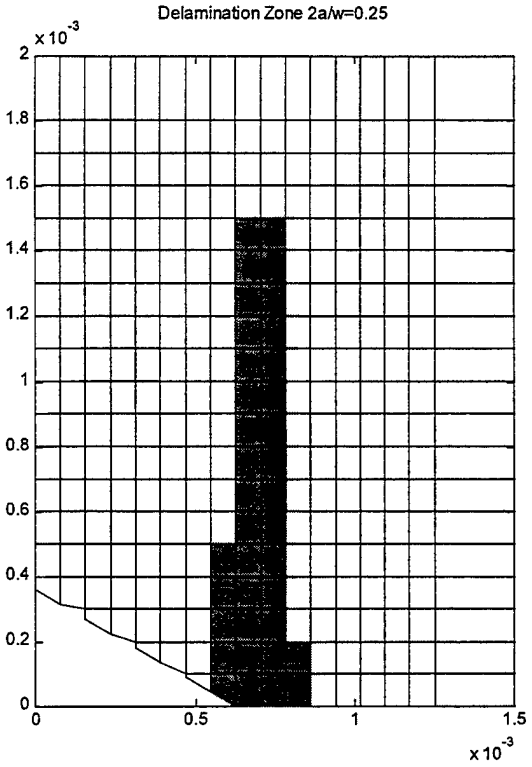

Figure 19 Delamination Zone w=5mm

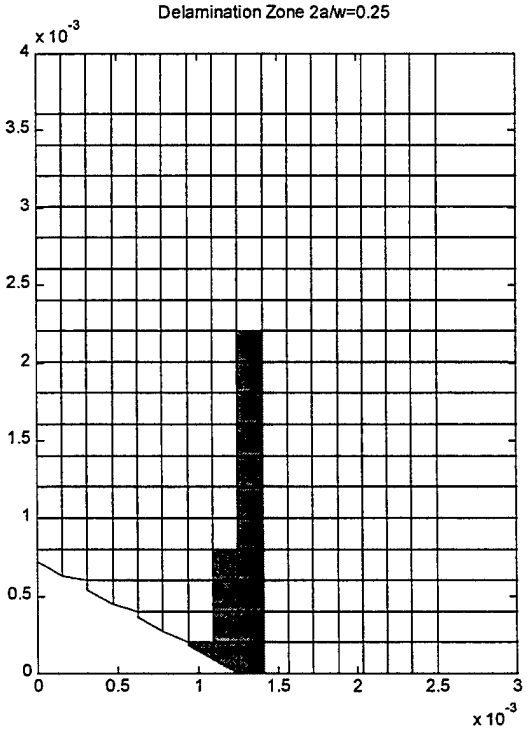

Figure 20 Delamination Zone w=10mm

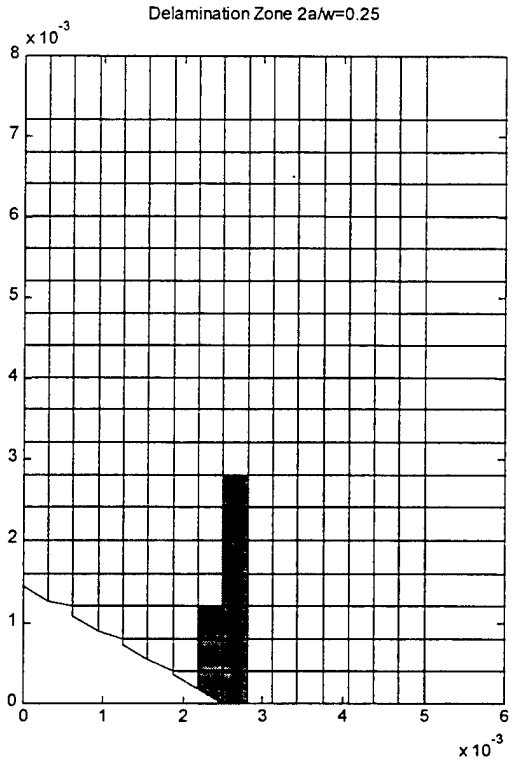

Figure 21 Delamination Zone w=20mm

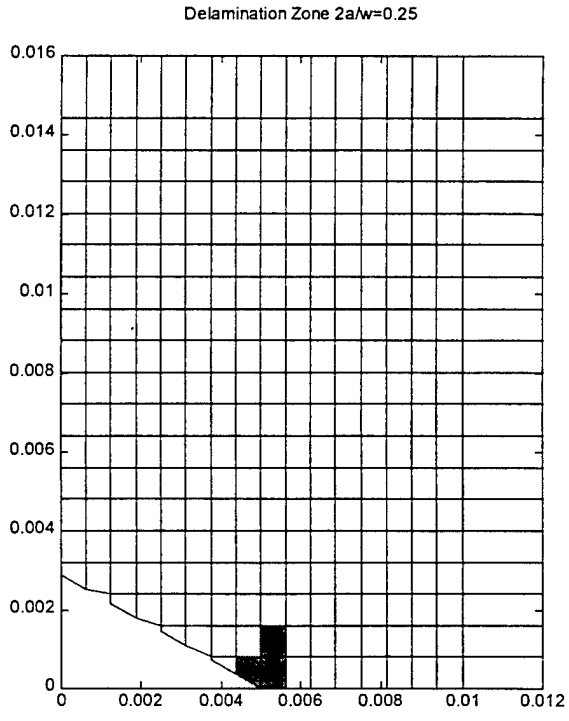

Figure 22 Delamination Zone w=40mm

IV. CONCLUSIONS AND RECOMMENDATIONS

The combined micro- and macromechanical approach to analysis of composite materials is an effective method of exploring and simulating the initiation of damage. It efficiently enables the incorporation of constituent homogeneous material behavior into analysis of heterogeneous materials. In this work micro-/macromechanical analysis was used to simulate each of the three experimentally observed modes of failure for DEN cross-ply fibrous composites. A thin layer of homogeneous matrix elements was necessary to properly model observed delamination behavior. The delamination layer made the transmission of stresses and damage across the laminar boundaries conveniently observable. The quadratic delamination criterion applied to delamination layer elements did correctly predict delamination zone shape for a variety of geometries. Proper mesh refinement is necessary to correctly simulate specimen behavior in the vicinity of the notch tip.

Future research in this area should include both experimental and simulated examinations of multi-axial loading. This work examined failure modes that occurred exclusively in the matrix regions; incorporation of fiber failure and degradation should be included in future work.

LIST OF REFERENCES

1. Kortschot, M. T., and Beaumont, P. W. R., "Damage Mechanics of Composite Materials: I—Measurements of Damage and Strength," *Composites Science and Technology*, Vol. 39, pp. 289-301, 1990.

2. Chen, D. J., Chan, W. S., and Wang, B. P., "Efficient Method to Simulate One- and Two-Dimensional Delamination Growth in Composite Laminates," *Journal of Reinforced Plastics and Composites*, Vol. 15, pp. 944-957, 1996.

3. Hitchings, D., Robinson, P., and Javidrad, F., "Finite Element Model for Delamination Propagation in Composites," *Computers and Structures*, Vol. 60, pp. 1093-1104, 1996.

4. Davidson, B. D., Hu, Hurang, and Schapery, R. A., "Analytical Crack-Tip Element for Layered Elastic Structures," *Journal of Applied Mechanics*, Vol. 62, pp. 294-305, 1995.

5. Reedy, E. D., Jr., Mello, F. J., and Guess, T. R., "Modeling the Initiation and Growth of Delaminations in Composite Structures," *Journal of Composite Materials*, Vol. 31, pp. 812-831, 1997.

6. Brewer, J. C., and Lagace, P. A., "Quadratic Stress Criterion for Initiation of Delamination," *Journal of Composite Materials*, Vol. 22, pp. 1141-1155, 1988.

7. Kassapoglou, C., and Lagace, P. A., "An Efficient Method for the Calculation of Interlaminar Stresses in Composite Materials," *Journal of Applied Mechanics*, Vol. 53, pp. 744-750, 1986.

8. Ardic, E. S., Bolcan, C., and Kayran, A., "Method of Strain and Stress Analysis for Failure Prediction in Laminated Composites," *Proceedings of the Institution of Mechanical Engineers, Part G: Journal of Aerospace Engineering*, Vol. 209, pp. 43-51, 1995.

9. Zhu, H., Sankar, B. V., and Marrey, R. V., "Evaluation of Failure Criteria for Fiber Composites Using Finite Element Micromechanics," *Journal of Composite Materials*, Vol. 32, pp. 766-782, 1998.

10. Jones, R. M., Mechanics of Composite Materials, Hemisphere Publishing Corporation, New York, p. 87.

11. Halpin, J. C., *Primer on Composite Materials: Analysis*, Technomic Publishing Company, Inc., Lancaster, PA, pp. 130-142, 1984.

12. Aboudi, J., Mechanics of Composite Materials: A Unified Micromechanical Approach, Elsevier, New York, pp. 35-53, 1991.

13. Pecknold, D. A., "A Framework for 3-D Nonlinear Modeling of Thick-Section Composites," DTRC-SME-90/92, *Ship Materials Engineering Department Research and Development Report*, David Taylor Research Center, 1992.

14. Kwon, Y.W., "Calculation of Effective Moduli of Fibrous Composites with Micro-Mechanical Damage," *Composite Structures*, Vol 25, pp. 187-192, 1993.

15. Kwon, Y. W., "Material Nonlinear Analysis of Composite Plate Bending using New Finite Element Formulation," *Computers & Structures*, Vol. 41, No. 5, pp. 1111-1117, 1991.

16. Kwon, Y. W., and Byun, K. Y., "Development of a New Finite Element Formulation for the Elasto-Plastic Analysis of Fiber-Reinforced Composites," *Computers & Structures*, Vol. 35, No. 5, pp. 563-570, 1990.

17. Kwon, Y. W., "Thermo-Elastoviscoplastic Finite Element Plate Bending Analysis of Composites." *Engineering Computations*, Vol. 9, pp. 595-607, July 1992.

18. Kwon, Y. W., and Berner, J. M., "Micromechanics Model for Damage and Failure Analyses of Laminated Fibrous Composites," *Engineering Fracture Mechanics*, Vol. 52, No. 2, pp. 231-242, 1995.

19. Kwon, Y. W., and Kim, C., "Micromechanical Model for Thermal Analysis of Particulate and Fibrous Composites," *Journal of Thermal Stresses*, Vol. 21, pp. 21-39, 1998.

20. Kwon, Y. W., and Liu, C. T., "Study of Damage Evolution in Composites Using Damage Mechanics and Micromechanics," *Composite Structures*, Vol. 38, pp. 133-139, 1997.

21. Ugural, A. C., and Fenster, S. K., *Advanced Strength and Applied Elasticity*, Prentice Hall PTR, Upper Saddle River, NJ, pp. 15-17, 1993.

22. Kwon, Y. W., and Bang, H., *The Finite Element Method Using MATLAB*, CRC Press, Boca Raton, 1997.

23. Akin, J. E., Application and Implementation of Finite Element Methods, Academic Press, Inc., New York, 1982.

INITIAL DISTRIBUTION LIST

1. Defense Technical Information Center 2
   8725 John J. Kingman Rd., STE 0944
   Ft. Belvoir, Virginia 22060-6218

2. Dudley Knox Library 2
   Naval Postgraduate School
   411 Dyer Rd.
   Monterey, CA 93943-5101

3. Professor Young W. Kwon, Code ME/Kw 2
   Department of Mechanical Engineering
   Naval Postgraduate School
   Monterey, CA 93943

4. Department Chairman, Code ME 1
   Department of Mechanical Engineering
   Naval Postgraduate School
   Monterey, CA 93943

5. Naval Engineering Curricular Office (Code 34) 1
   Naval Postgraduate School
   Monterey, CA 93943

6. LT Linda E. Craugh 1
   209 Fox Drive
   Mechanicsburg, PA 17055-2534